Aerospace Science and Technology 45 (2015) 387–397

Contents lists available at ScienceDirect

Aerospace Science and Technology

www.elsevier.com/locate/aescte

4D trajectory estimation based on nominal flight profile extraction and airway meteorological forecast revision

Xinmin Tang [a,b,c,*], Ping Chen [b], Yu Zhang [c]

[a] College of Civil Aviation, Nanjing Aeronautics and Astronautics University, Nanjing 211106, China
[b] China Electronics Technology Group Corporation, 28th, Nanjing 210007, China
[c] Civil and Environmental Engineering, University of South Florida, Tampa 33620, USA

ARTICLE INFO

Article history:
Received 25 January 2015
Received in revised form 29 April 2015
Accepted 2 June 2015
Available online 6 June 2015

Keywords:
Air traffic control automation system
Four-dimensional trajectory estimation
Flight profile extraction
Meteorological forecast revision

ABSTRACT

To address the problem of high accuracy strategic four-dimensional (4D) trajectory estimation for air traffic control automation systems, we proposed a method for extracting the nominal flight profile and revising airway meteorological forecasts. First, for extracting flight intention from historical Aircraft Meteorological Data Relay (AMDAR) data, a Dynamic Space Warping (DSW) algorithm is applied to measure the distance between two flight altitude profiles, where the nominal flight altitude profile is regarded as that with the DSW distance nearest to others. To eliminate the influence of meteorological factors, ground speed calculation is combined with the CAS/TAS conversion model to extract the nominal flight airspeed profile. By considering the meteorological forecast error from GRIdded Binary (GRIB) data, Cressman interpolation is employed to revise the original forecasts from GRIB data combined with observations from new AMDAR data relayed by another reference aircraft, which can be used for strategic 4D trajectory estimation for object aircraft. We present a case study to demonstrate that the nominal flight profile obtained reflects flight intention and it eliminates the influence of meteorological factors, while the airway meteorological model provides more accurate meteorological forecasts for strategic 4D trajectory estimation.

1. Introduction

Due to the rapid speed development of civil aviation, it is difficult to ease the air traffic pressure by using imprecise intervals for aircraft to prevent air traffic congestion. Thus, the United States and Europe are employing next generation air traffic management systems based on four-dimensional (4D) trajectory operation, which are called the Next Generation Air Transportation System (NextGen) and Single European Sky (SESAR), respectively. The Civil Aviation Administration of China (CAAC) also started planning the development of a new generation air traffic management system in 2007, which is expected to be completed in 2025. Similar as in the systems in the U.S. and Europe, one of the key techniques for improving the efficiency of air traffic and reducing emission and pollution is 4D trajectory-based operation (4D TBO) [1].

In recent years, most studies of 4D trajectory prediction around the world have paid close attention to building aircraft operation models, where they usually assume that a flight profile comprises several phases, the aim of these studies is to establish accurate dynamics or kinematics equations for each phase. R. Slattery [2] proposed a trajectory generation algorithm for radar control automation system. In this algorithm, the flight trace is connected via the designated points with straight lines or arcs, and the vertical flight profile is divided into a series of flight segments where the second-order Runge–Kutta method is used to generate the trajectory. Wu [3] studied a numerical integral algorithm and a simplified algebraic algorithm for calculating flight profiles in terminal areas, but it did not consider meteorological factors and flight intention. Richard [4] studied the impact of airline flight-planning data on the Center TRACON Automation System (CTAS) in terms of the en route climb trajectory prediction accuracy. First, the climb trajectory synthesis process is described with existing input data. The flight-planning data parameters available from a typical airline operations center are then considered as well as their potential usefulness to CTAS. Chester [5] proposed a method that employed a climbing timetable from the flight performance manual to obtain aerodynamic models and the aircraft dynamic equations for flight trajectory estimation. Wang et al. [6] and Tang et al. [7] divided the flight phase according to the characteristics of flight models, however their methods are too ideal to obtain specific kinetic parameters during actual flights, and the ideal phase division does not necessarily conform to the real operations. Moreover, the

* Corresponding author at: 29 Jiangjun St, Nanjing, China. Tel.: +86 13813952160.
E-mail address: tangxinmin@nuaa.edu.cn (X. Tang).

http://dx.doi.org/10.1016/j.ast.2015.06.001
1270-9638/

flight intention should also be considered. Krozel [8] proposed a method for inferring the intention and structured a process for obtaining the best fit to an intent model for observed aircraft motions, where the horizontal, vertical, and speed dimensions were investigated independently, and then combined to fully explain the three-dimensional guidance and navigation plan of an aircraft. Yepes [9] used a hybrid estimation algorithm to estimate the aircraft's state and flight mode, these estimates were then combined with the knowledge of air traffic control regulations, the aircraft's flight plan, and the environment to infer the pilot's intention. The trajectory predictions are computed as a function of the aircraft's motion and the inferred intention. Konyak [10] used the Target Generation Facility (TGF) trajectory predictor and the TGF simulator to demonstrate that Aircraft Intent Description Language (AIDL) can be used to interchange aircraft intent information with a trajectory predictor and the predicted and simulated trajectories are compatible. Some researchers have also tried to predict 4D trajectories using historical flight data. Wu et al. [11] forecasted the time of arrival based on mining historical flight time data, nevertheless, their study did not identify flight profiles despite employing meteorological data and the control intention. Gariel et al. [12] employed the K-means clustering algorithm to analyze the trajectories in a terminal area based on radar data, but their method was difficult to be applied for obtaining the entire flight profile. Eurocontrol [13] defined the standard airline procedures in the Base of Aircraft Data (BADA) to provide a method for simulating standard or nominal aircraft operations for various air traffic management applications, but the BADA airline procedure model only identifies the possibility of introducing notion of different altitude altimetry readings to calculate the calibrated air speed schedules in user applications. Therefore, the aircraft operation varies significantly in function of specific airspace procedures and operating policies of locally dominant airlines, and thus the resulting speed schedules of the standard airline procedure model may differ and they are difficult to define uniformly.

Furthermore, meteorological factors play roles in accuracy of 4D trajectory prediction. Tino et al. [14] demonstrated that the spatial distribution of errors in wind forecasts played a significant role in trajectory prediction based on a statistical analysis of the Rapid Update Cycle (RUC-2) wind forecasts and by comparing the forecast with one year of archived Aircraft Communications Addressing and Reporting System (ACARS) wind speed observations. Zheng et al. [15] proposed a statistical model of wind forecast uncertainty for stochastic trajectory generations based on the errors in previous wind forecasts obtained from the RUC weather prediction system. Reynolds et al. [16] quantified the relationship between the quality of wind information and the benefits of the future applications envisioned for NextGen, including the impacts of wind information accuracy on 4D-TBO performance in terms of required time of arrival compliance and fuel burn. Weitz [17] noted that the most important factors for trajectory prediction are meteorological parameters (wind and temperature), aircraft performance (weight and speed), and navigation performance. To investigate the effect of parametric errors, a simulation was implemented with over 2000 flights in various environmental conditions. Zhu et al. [18] introduced the concept of virtual observation waypoints by using a statistical prediction system based on a Kalman filter, and by combining information from Aircraft Meteorological Data Relay (AMDAR) data with World Area Forecast System (WAFS) GRIdded Binary (GRIB) forecast data. The model can significantly improve the resolution and accuracy of meteorological forecasts along the airway, but it is not suitable for a scenario where the airway of the reference aircraft relayed AMDAR differs from that of the object aircraft.

To extract flight intention from historical trajectories, we propose a method that uses historical AMDAR data to generate a nominal flight profile, without depending on dynamics or kinematics models and eliminating the influence of meteorological factors. Given the fact that the 4D trajectory estimation of an object aircraft is influenced by meteorological factors, we employ Cressman interpolation to revise the original forecasts from GRIB data, which we combine with observations obtained from new AMDAR data to improve the accuracy of 4D trajectory estimation.

Table 1
Frequency of observations in different flight stages.

Flight stages	Observation interval
Climb (0–1400 m)	6 s
Climb (1400–6000 m)	20 s
Cruise	180 s
Descent	60 s

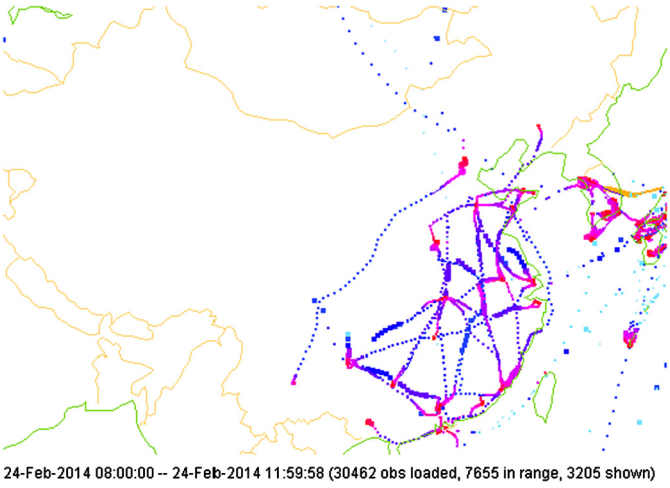

Fig. 1. Distribution of AMDAR data in China.

2. Description of AMDAR and GRIB data

2.1. Characteristics of AMDAR data

AMDAR is a meteorological observation program, which is being promoted worldwide by the International Civil Aviation Organization (ICAO) and World Meteorological Organization (WMO). AMDAR uses commercial aircraft to collect atmospheric data and relay them back to the ground via ACARS data link. In 2004, the AMDAR program began to participate in data exchange with the Global Telecommunication System (GTS) in China, which is a part of China's AMDAR project, where the partial completion of data acquisition and transmission has been achieved [19].

The meteorological observations relayed by commercial aircraft include the observation time τ_{OBS}, longitude l_{OBS}, latitude b_{OBS}, altitude h_{OBS}, air temperature t_{OBS}, north wind component u_{OBS} and east wind component v_{OBS}. From the perspective of aircrafts, the AMDAR data can be treated as their historical trajectories, including meteorological factors, flight intention.

The frequencies of the observations made during each flight stage are shown in Table 1. Obviously, the frequency is much higher during the climb or descent stages than during the cruise stage, especially when climbing from 0 to 1400 m. Fig. 1 shows the distribution of AMDAR data in China at 08:00–12:00 on February 24, 2014 based on 30 462 observations.

The AMDAR program is still in its infancy and it is restricted by the airways, so the AMDAR data are concentrated mainly in the

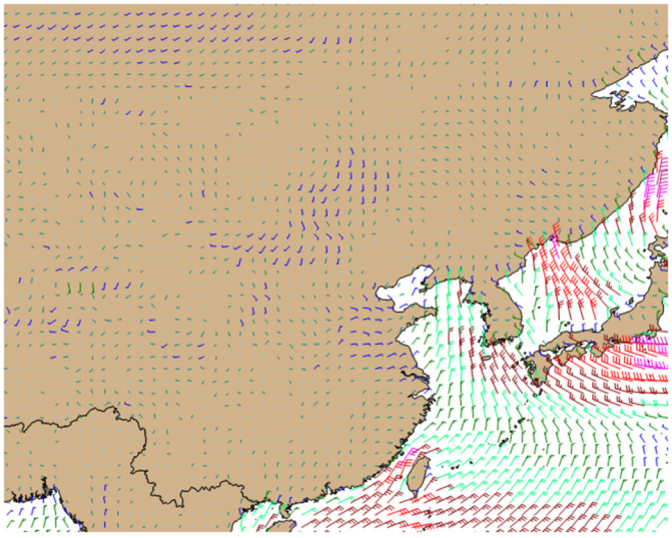

Fig. 2. Distribution of GRIB data in China.

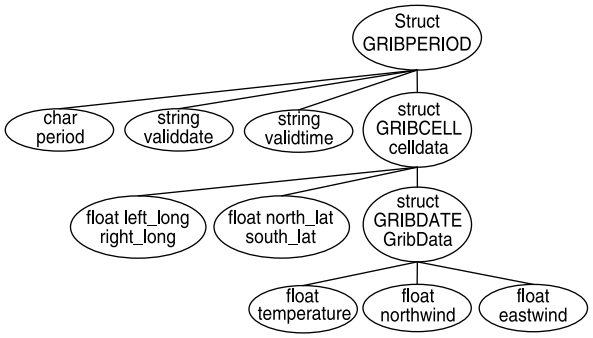

Fig. 3. Structure of simplified GRIB data.

eastern region of China at present, including Beijing, Guangzhou and Shanghai.

2.2. Characteristics of GRIB data

GRIB is a concises data format used widely in meteorology to store historical and forecast weather data. The first edition is used worldwide by most meteorological centers for Numerical Weather Prediction (NWP) output. A new generation has been introduced, known as GRIB second edition, and the data are slowly being changed over to this format. GRIB data provides 1/3/5/7-days meteorological forecasts and it is updated every 3/6/12/24 hours, respectively. For each forecasting interval, the meteorological factors are provided at 37 pressure levels with a resolution of $0.5^\circ \times 0.5^\circ$, as shown in Fig. 2.

A GRIB data comprises a self-describing data objects, i.e., each record contains the data, but also the metadata that describes the spatial grid, the valid time, and any ensemble metadata. GRIB data may be concatenated together to form a single dataset, but each record is self-describing and the order in which they may be merged is arbitrary. The data structure for simplified GRIB data is shown in Fig. 3, where the element Celldata records the longitude l_{FST} to forecast and the latitude b_{FST} to forecast and the compound element GribData records the air temperature forecast t_{FST} and wind vector forecast, including north wind component u_{FST} and east wind component v_{FST}.

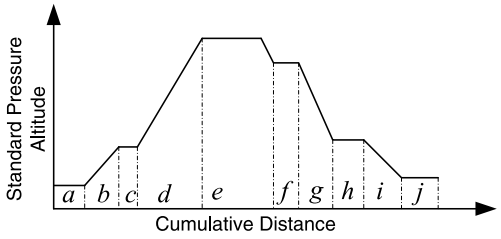

Fig. 4. Diagram showing a typical flight altitude profile.

3. Extracting the nominal flight profile

3.1. Extracting the nominal altitude profile

The flight altitude profile refers to a two-dimensional image that describes the relationship between the flight altitude and flight distance, i.e., the trajectory in the vertical direction. A typical flight altitude profile comprises three stages as shown in Fig. 4, where $a \sim d$ represents the climbing stage, e and f denote the cruise stage, and $g \sim j$ is the descent stage. The specific altitude parameters for each stage can be found in [20].

Altitude profiles cannot be exactly the same because the flight intentions differ even for the same flight on a different day. In our proposed method, we eliminate the randomness from historical flight altitude profiles to obtain a representative altitude profile, which is called the nominal flight altitude profile.

Let $M = \{P_1, P_2, \ldots, P_S\}$ be the set of S historical flight altitude profiles for the same flight acquired from AMDAR data, and the i-th profile $P_i = \{p_i^1, p_i^2, \ldots, p_i^k\}$ comprises k historical samples. Let $p_i^j \in H \times D$ be an arbitrary sample, where j is the sample index, and $H \subset \mathrm{R}$ denotes the flight altitude domain, and $D \subset \mathrm{R}$ denotes the flight distance domain. The order of all samples is determined by distance, and thus for two samples $\forall p_i^m \ (h_i^m, d_i^m) \in P_i$ and $\forall p_i^n \ (h_i^n, d_i^n) \in P_i$ from a profile, if $m > n$, then $d_i^m > d_i^n$.

According to the characteristics of the historical flight profiles, the Euclidean distance cannot be used to calculate the distance between flight altitude profiles. The Dynamic Time Warping (DTW) algorithm [21,22] is a typical method that is employed to compute the likelihood of similarity between unsynchronized time series or those with different lengths. Similarly, for the same flight, the flight range could not be exactly the same every time, we suppose that the distance dimension can be stretched and scaled locally, so we propose a Dynamic Space Warping (DSW) algorithm, where the distance domain is stretched or compressed to achieve a reasonable fit.

Let $P_1 = \{(h_{\mathrm{OBS},1}^1, d_{\mathrm{OBS},1}^1), (h_{\mathrm{OBS},1}^2, d_{\mathrm{OBS},1}^2), \ldots, (h_{\mathrm{OBS},1}^m, d_{\mathrm{OBS},1}^m)\}$ and $P_2 = \{(h_{\mathrm{OBS},2}^1, d_{\mathrm{OBS},2}^1), (h_{\mathrm{OBS},2}^2, d_{\mathrm{OBS},2}^2), \ldots, (h_{\mathrm{OBS},2}^n, d_{\mathrm{OBS},2}^n)\}$ be two altitude profiles for the same flight at different times, where the number of samples is m and n, respectively. The process involved in searching the warping path can be described as how to match two samples from each altitude profiles.

Construct an $m \times n$ matrix $\boldsymbol{A}_{m\times n}$, which includes the element a_{ij},

$$a_{ij} = \sqrt{\left(h_{\mathrm{OBS},2}^i - h_{\mathrm{OBS},1}^j\right)^2} \tag{1}$$

where a_{ij} is the distance between samples $p_1^j \in P_1$ and $p_2^i \in P_2$. As shown in Fig. 5, the warping path $W = \{w_1, w_2, \ldots, w_k\}$ is contained in matrix $\boldsymbol{A}_{m\times n}$, and the DSW distance between P_1 and P_2 is calculated by

$$d_{\mathrm{DSW}}(P_1, P_2) = \min\left\{\frac{1}{k}\sum_{i=1}^{K} w_i\right\}, \tag{2}$$

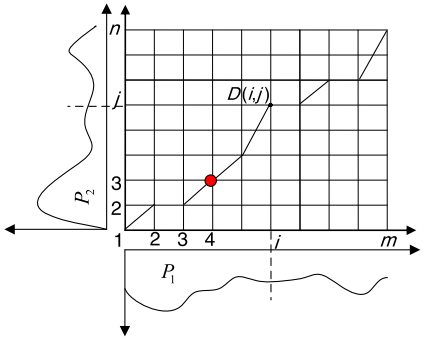

Fig. 5. Diagram showing the dynamic space warping algorithm.

$$\text{s.t.}\begin{cases} m+n-1 \geq K > \max\{m,n\} & (1)\\ w_1 = a_{11}, \quad w_K = a_{mn} & (2)\\ w_k = a_{ij}, \quad w_{k-1} = a_{uv},\ 0 \leq i-u \leq 1,\ 0 \leq j-v \leq 1, & (3)\end{cases} \tag{3}$$

where (1) represents the warping path length constraint, (2) represents the warping path beginning and ending constraint, and (3) represents the continuity constraint.

Dynamic programming can be used to search for the warping path with the minimum cumulative distance. For two altitude profiles, P_1 and P_2, the dynamic programming equation and boundary condition used to search for the warping path are as follow.

$$\begin{cases} f(i,j) = a_{ij} + \min\{f(i-1,j-1), f(i,j-1), f(i-1,j)\} \\ f(1,1) = a_{11} \end{cases} \tag{4}$$

Finally, the distance between the two flight altitude profiles $d_{\mathrm{DSW}}(p_1,p_2) = f(m,n)$ can be achieved by computing the recursive Equation (4).

Suppose that there are S flight altitude profiles $M = \{P_1, P_2, \ldots, P_S\}$ for the same flight, then the nominal flight altitude profile $P_{\mathrm{NOM}} \in M$ is defined as that where the mean DSW distance is the nearest relative to others, i.e.,

$$\sum_{j=1}^{S} d_{\mathrm{DSW}}(P_{\mathrm{NOM}}, P_j) \leq \sum_{j=1}^{S} d_{\mathrm{DSW}}(P_i, P_j), \quad \forall P_i \in M. \tag{5}$$

Thus the fitting degree $\gamma(P_{\mathrm{NOM}})$ for nominal flight altitude profile can be calculated by

$$\gamma(P_{\mathrm{NOM}}) = 100\% - \frac{\sum_{j=1}^{S} d_{\mathrm{DSW}}(P_{\mathrm{NOM}}, P_j)}{\sum_{i=1}^{S}\sum_{j=1}^{S} d_{\mathrm{DSW}}(P_i, P_j)}. \tag{6}$$

3.2. Extracting the nominal airspeed profile

The flight airspeed profile is a two-dimensional image that describes the relationship between airspeed and flight distance. A typical flight airspeed profile comprises a series of states, as shown in Fig. 6, where a represents a take-off and acceleration state, b is a climbing state with constant calibrated airspeed, c is a state that accelerates to cruising speed, d is a cruising state with constant calibrated airspeed or Mach number, e is a decelerating state, f is a descending state based on calibrated air speed, and g is a decelerating state for landing.

The intended flight cannot have same flight airspeed profile, even for the same flight on a different day. Thus, our purposed method eliminates the randomness from flight airspeed profiles as well as finding a representative airspeed profile, which is called the nominal flight airspeed profile and represented by $S_{\mathrm{NOM}} = \{s^1_{\mathrm{NOM}}, s^2_{\mathrm{NOM}}, \ldots, s^k_{\mathrm{NOM}}\}$, where $s^j_{\mathrm{NOM}} \in C \times D$ denotes an arbitrary sample, $C \subset \mathrm{R}$ denotes the calibrated airspeed domain, and $D \subset \mathrm{R}$ denotes the flight distance domain.

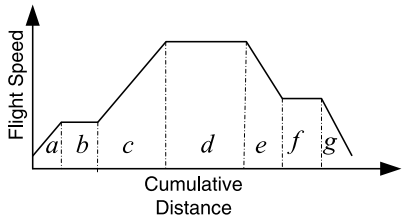

Fig. 6. Diagram showing a typical flight speed profile.

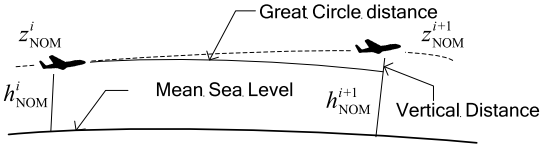

Fig. 7. Diagram showing the great circle distance.

Before extracting the airspeed profile, the ground speed needs to be evaluated first. The historical AMDAR data relayed by the aircraft does not contain ground speed information, so the ground speed can only be calculated based on the great circle distance between two waypoints.

Let $P_{\mathrm{NOM}} = \{p^1_{\mathrm{NOM}}, p^2_{\mathrm{NOM}}, \ldots, p^k_{\mathrm{NOM}}\}$ be the nominal altitude profile, $p^i_{\mathrm{NOM}}(h^i_{\mathrm{NOM}}, d^i_{\mathrm{NOM}}) \in P_{\mathrm{NOM}}$ and $p^{i+1}_{\mathrm{NOM}}(h^{i+1}_{\mathrm{NOM}}, d^{i+1}_{\mathrm{NOM}}) \in P_{\mathrm{NOM}}$ be two adjacent samples, the location of one observing waypoint p^i_{NOM} at time τ^i_{NOM} be $z^i_{\mathrm{NOM}}(l^i_{\mathrm{NOM}}, b^i_{\mathrm{NOM}}, h^i_{\mathrm{NOM}})$ and the next one p^{i+1}_{NOM} at time $\tau^{i+1}_{\mathrm{NOM}}$ be $z^{i+1}_{\mathrm{NOM}}(l^{i+1}_{\mathrm{NOM}}, b^{i+1}_{\mathrm{NOM}}, h^{i+1}_{\mathrm{NOM}})$, and the meteorological factors for each waypoint be $m^i_{\mathrm{NOM}}(u^i_{\mathrm{NOM}}, v^i_{\mathrm{NOM}}, t^i_{\mathrm{NOM}})$ and $m^{i+1}_{\mathrm{NOM}}(u^{i+1}_{\mathrm{NOM}}, v^{i+1}_{\mathrm{NOM}}, t^{i+1}_{\mathrm{NOM}})$, as shown in Fig. 7.

Considering the altitude difference between waypoint z^i_{NOM} and z^{i+1}_{NOM}, the aircraft ground speed from one waypoint to another can be decomposed into two components, i.e., the horizontal ground speed $\vec{v}^i_{\mathrm{GS}}$ and the vertical climb or descent speed $\vec{v}^i_{\mathrm{VS}}$, which can be calculated by

$$\begin{cases} v^i_{\mathrm{GS}} = \dfrac{d^{i+1}_{\mathrm{NOM}} - d^i_{\mathrm{NOM}}}{\tau^{i+1}_{\mathrm{NOM}} - \tau^i_{\mathrm{NOM}}} \\ v^i_{\mathrm{VS}} = \dfrac{|h^{i+1}_{\mathrm{NOM}} - h^i_{\mathrm{NOM}}|}{\tau^{i+1}_{\mathrm{NOM}} - \tau^i_{\mathrm{NOM}}}, \end{cases} \tag{7}$$

where the great circle distance can be calculated by

$$\begin{cases} d^{i+1}_{\mathrm{NOM}} - d^i_{\mathrm{NOM}} = \left(R_{\mathrm{ME}} + \min\{h^i_{\mathrm{NOM}}, h^{i+1}_{\mathrm{NOM}}\}\right) \cdot \varphi^{i,i+1}_{\mathrm{NOM}} \\ \varphi^{i,i+1}_{\mathrm{NOM}} = \cos^{-1}\left[\cos\left(b^i_{\mathrm{NOM}}\right) \cdot \cos\left(b^{i+1}_{\mathrm{NOM}}\right) \cdot \cos\left(l^i_{\mathrm{NOM}} - l^{i+1}_{\mathrm{NOM}}\right)\right. \\ \qquad\qquad \left. + \sin\left(b^i_{\mathrm{NOM}}\right) \cdot \sin\left(b^{i+1}_{\mathrm{NOM}}\right)\right], \end{cases} \tag{8}$$

where R_{ME} represents the mean earth radius. As a result, the true airspeed v^i_{TAS} can be calculated easily based on the flight speed triangle which comprises three vectors, as shown in Fig. 8: the ground speed vector $\vec{v}^i_{\mathrm{GS}}$, the true airspeed vector $\vec{v}^i_{\mathrm{TAS}}$, and the wind speed vector $\vec{v}^i_{\mathrm{WS}}$, where $\vec{v}^i_{\mathrm{WS}} = (u^i_{\mathrm{OBS}}, v^i_{\mathrm{OBS}})$ is a wind speed vector acquired from AMDAR data, ε_i is the drift angle, and α_i is the wind angle.

According to the resultant vector principle, the true airspeed can be calculated by

$$v^i_{\mathrm{TAS}} = \frac{v^i_{\mathrm{GS}} - ((u^i_{\mathrm{NOM}})^2 + (v^i_{\mathrm{NOM}})^2)^{1/2} \cdot \cos\alpha_i}{\cos\varepsilon_i}. \tag{9}$$

According to the transition relation between calibrated airspeed v^i_{CAS} and true airspeed v^i_{TAS} based on the CAS/TAS conversion

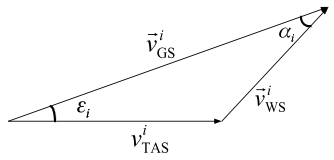

Fig. 8. Diagram showing the flight speed triangle.

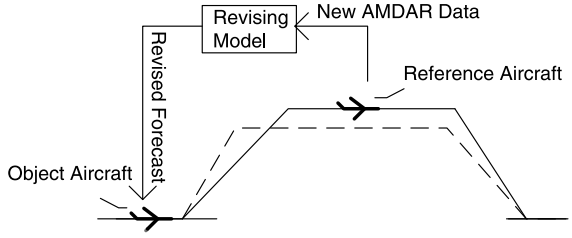

Fig. 9. Revision of airway meteorological factors.

model [13], we can obtain the nominal calibrated airspeed profile $S_{NOM} = \{(v^1_{CAS}, d^1_{NOM}), (v^2_{CAS}, d^2_{NOM}), \ldots, (v^i_{CAS}, d^i_{NOM}), \ldots\}$:

$$v^i_{CAS} = 1479.1 \times \left(\left(\delta_i \cdot \left(\left(\frac{t_{MSL}}{t^i_{NOM}}\left(\frac{v^i_{TAS}}{1479.1}\right)^2 + 1\right)^{3.5} - 1\right) + 1\right)^{1/3.5} - 1\right)^{1/2}, \tag{10}$$

where t_{MSL} is the standard atmospheric temperature at mean sea level (MSL), t^i_{NOM} is the air temperature at the aircraft's location, which is acquired from AMDAR data, and

$$\delta_i = \begin{cases} (1 - 6.87559 \times h^i_{NOM})^{5.25588}, & h^i_{NOM} \le 36\,089 \text{ ft} \\ 0.2233609 \times \exp(\frac{36089 - h^i_{NOM}}{20805.8}), & h^i_{NOM} > 36\,089 \text{ ft}. \end{cases} \tag{11}$$

4. High accuracy strategic 4D trajectory estimation

4.1. Airway meteorological forecast revision

We proposed an airway meteorological forecast revision model to improve the meteorological forecast accuracy by combining GRIB data and new AMDAR data, as shown in Fig. 9. It is supposed that the departing time difference between the reference aircraft and the object aircraft is less than the updating interval of the GRIB data. The meteorological observations acquired from new AMDAR data relayed by the reference aircraft can be used to revise the meteorological forecasts acquired from GRIB data related to the object aircraft, and the revised forecasts can be then used to calculate the airway meteorological factors for the object aircraft.

We employ an interpolation method called Cressman interpolation, which is used widely in the meteorological field. As shown in Fig. 10, we arbitrarily select a tridimensional grid with eight vertices $M_i(l^M_i, b^M_i, h^M_i)$, $i = 1, 2, \ldots, 8$ from the original GRIB data, which contains sufficient observation waypoints $N_j(l^N_j, b^N_j, h^N_j)$, $j = 1, 2, \ldots$ from new AMDAR data relayed by the reference aircraft.

According to Cressman interpolation [23], the meteorological forecast $\boldsymbol{\alpha}(M_i) = [t^{M_i}_{FST}, u^{M_i}_{FST}, v^{M_i}_{FST}]^T$ for M_i is revised as follows:

$$\boldsymbol{\alpha}'(M_i) = \boldsymbol{\alpha}(M_i) + \Delta\boldsymbol{\alpha}(M_i), \tag{12}$$

where $\boldsymbol{\alpha}(M_i)$ is the forecast for M_i and $\Delta\boldsymbol{\alpha}(M_i) = [\Delta t^{M_i}_{FST}, \Delta u^{M_i}_{FST}, \Delta v^{M_i}_{FST}]^T$ is the forecast error for M_i calculated by

$$\Delta\boldsymbol{\alpha}(M_i) = \frac{\sum_{i=1}^{k} W_{ij} \cdot \Delta\boldsymbol{\alpha}(N_j)}{\sum_{i=1}^{k} W_{ij}}, \tag{13}$$

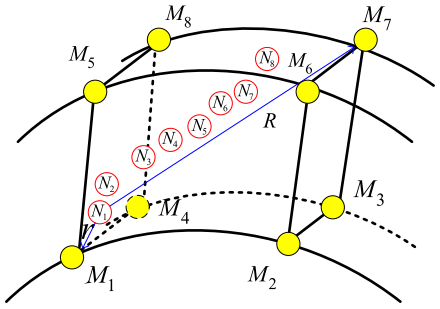

Fig. 10. A tridimensional grid with eight vertices.

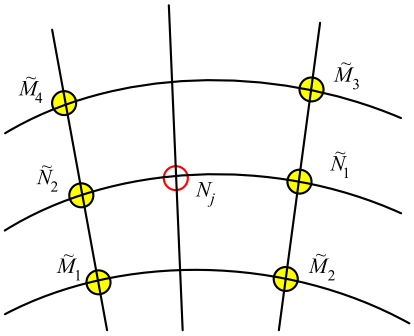

Fig. 11. Virtual vertices at pressure level h^N_j.

where W_{ij} represents a weighting factor determined by the Euclidean distance r_{ij} from M_i to N_j and the scanning radius R, while

$$W_{ij} = \begin{cases} \frac{R^2 - r^2_{ij}}{R^2 + r^2_{ij}}, & r_{ij} \le R \\ 0, & r_{ij} > R, \end{cases} \tag{14}$$

and $\Delta\boldsymbol{\alpha}(N_j)$ is the difference between observation $\boldsymbol{\beta}(N_j) = [t^{N_j}_{OBS}, u^{N_j}_{OBS}, v^{N_j}_{OBS}]^T$ for N_j from the new AMDAR data and the forecast $\boldsymbol{\alpha}(N_j) = [t^{N_j}_{FST}, u^{N_j}_{FST}, v^{N_j}_{FST}]^T$. N_j is not any vertex in the tridimensional grid, so $\boldsymbol{\alpha}(N_j)$ must be calculated via linear interpolation of the meteorological forecast.

As shown in Fig. 11, four virtual vertices $\tilde{M}_k(l_k = l^M_i = l^M_{i+4}, b_k = b^M_i = b^M_{i+4}, h_k = h^N_j)$, $k = 1, 2, 3, 4$ should be constructed at the pressure level h^N_j where N_j is located.

The Meteorological forecast for four virtual vertices $\tilde{M}_k$, $k = 1, 2, 3, 4$ can be calculated by linear interpolation as follows.

$$\boldsymbol{\alpha}(\tilde{M}_k) = \boldsymbol{\alpha}(M_k) + \frac{h^M_{k+4} - h^N_j}{h^M_{k+4} - h^M_k} \cdot \big(\boldsymbol{\alpha}(M_{k+4}) - \boldsymbol{\alpha}(M_k)\big), \quad k = 1, 2, 3, 4 \tag{15}$$

Meteorological forecast for two virtual vertices, $\tilde{N}_1(l_1 = l^M_1 = l^M_5, b^N_j, h^N_j)$ and $\tilde{N}_2(l_2 = l^M_2 = l^M_6, b^N_j, h^N_j)$, with the same latitude at the pressure level h^N_j can be calculated via linear interpolation as follows.

$$\begin{cases} \boldsymbol{\alpha}(\tilde{N}_1) = \boldsymbol{\alpha}(\tilde{M}_2) + \dfrac{b_3 - b^N_j}{b_3 - b_2} \cdot \big(\boldsymbol{\alpha}(\tilde{M}_3) - \boldsymbol{\alpha}(\tilde{M}_2)\big) \\ \boldsymbol{\alpha}(\tilde{N}_2) = \boldsymbol{\alpha}(\tilde{M}_1) + \dfrac{b_4 - b^N_j}{b_4 - b_1} \cdot \big(\boldsymbol{\alpha}(\tilde{M}_4) - \boldsymbol{\alpha}(\tilde{M}_1)\big). \end{cases} \tag{16}$$

The forecast $\boldsymbol{\alpha}(N_j)$ for N_j then can be calculated by linear interpolation as

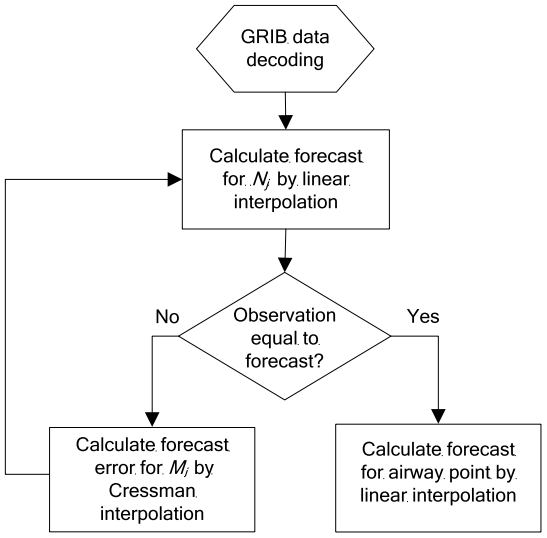

Fig. 12. Flowchart of airway meteorological forecast revision.

$$\boldsymbol{\alpha}(N_j) = \boldsymbol{\alpha}(\tilde{N}_1) + \frac{l_2 - l_j^N}{l_2 - l_1} \cdot \big(\boldsymbol{\alpha}(\tilde{N}_2) - \boldsymbol{\alpha}(\tilde{N}_1)\big). \tag{17}$$

After obtaining the revised meteorological forecasts for vertices M_i from the GRIB data, the meteorological forecasts $\boldsymbol{\alpha}(z^i_{\mathrm{NOM}}) = [t^i_{\mathrm{FST}}, u^i_{\mathrm{FST}}, v^i_{\mathrm{FST}}]^{\mathrm{T}}$ for any other waypoint $z^i_{\mathrm{NOM}}(l^i_{\mathrm{NOM}}, b^i_{\mathrm{NOM}}, h^i_{\mathrm{NOM}})$ from nominal fight altitude profile included in the tridimensional grid can be calculated via linear interpolation as

$$\boldsymbol{\alpha}\big(z^i_{\mathrm{NOM}}\big) = \boldsymbol{\alpha}'(\tilde{N}_1) + \frac{l_2 - l^i_{\mathrm{NOM}}}{l_2 - l_1} \cdot \big(\boldsymbol{\alpha}'(\tilde{N}_2) - \boldsymbol{\alpha}'(\tilde{N}_1)\big), \tag{18}$$

where

$$\begin{cases} \boldsymbol{\alpha}'(\tilde{M}_k) = \boldsymbol{\alpha}'(M_k) + \dfrac{h^M_{k+4} - h^i_{\mathrm{NOM}}}{h^M_{k+4} - h^M_k} \cdot \big(\boldsymbol{\alpha}'(M_{k+4}) - \boldsymbol{\alpha}'(M_k)\big), \\ \quad k = 1, 2, 3, 4 \\ \boldsymbol{\alpha}'(\tilde{N}_1) = \boldsymbol{\alpha}'(\tilde{M}_2) + \dfrac{b_3 - b^i_{\mathrm{NOM}}}{b_3 - b_2} \cdot \big(\boldsymbol{\alpha}'(\tilde{M}_3) - \boldsymbol{\alpha}'(\tilde{M}_2)\big) \\ \boldsymbol{\alpha}'(\tilde{N}_2) = \boldsymbol{\alpha}'(\tilde{M}_1) + \dfrac{b_4 - b^i_{\mathrm{NOM}}}{b_4 - b_1} \cdot \big(\boldsymbol{\alpha}'(\tilde{M}_4) - \boldsymbol{\alpha}'(\tilde{M}_1)\big). \end{cases} \tag{19}$$

A flowchart illustrating the airway meteorological forecast revision process is shown in Fig. 12.

4.2. Strategic 4D trajectory estimation

Given the nominal altitude profile $P_{\mathrm{NOM}} = \{p^1_{\mathrm{NOM}}, p^2_{\mathrm{NOM}}, \ldots, p^k_{\mathrm{NOM}}\}$ and nominal airspeed profile $S_{\mathrm{NOM}} = \{s^1_{\mathrm{NOM}}, s^2_{\mathrm{NOM}}, \ldots, s^k_{\mathrm{NOM}}\}$ for the object aircraft, as well as the revised airway meteorological forecasts $\boldsymbol{\alpha}(z^i_{\mathrm{NOM}}) = [t^i_{\mathrm{FST}}, u^i_{\mathrm{FST}}, v^i_{\mathrm{FST}}]^{\mathrm{T}}$, then the true airspeed for waypoint $z^i_{\mathrm{NOM}}(l^i_{\mathrm{NOM}}, b^i_{\mathrm{NOM}}, h^i_{\mathrm{NOM}})$ can be estimated by

$$v^i_{\mathrm{TAS}} = 1479.1 \times \left(\frac{t^i_{\mathrm{FST}}}{t_{\mathrm{MSL}}}\left(\left(1 + \frac{1}{\delta_j}\left(\left(1 + 0.2 \times \left(\frac{v^i_{\mathrm{CAS}}}{661.5}\right)^2\right)^{3.5} - 1\right)\right)^{1/3.5} - 1\right)\right)^{1/2}, \tag{20}$$

where

$$\delta_i = \begin{cases} (1 - 6.87559 \times 10^{-6} \times h^i_{\mathrm{NOM}})^{5.25588}, & h^i_{\mathrm{NOM}} \le 36\,089\ \mathrm{ft} \\ 0.2233609 \times \exp\left(\frac{36089 - h^i_{\mathrm{NOM}}}{20805.8}\right), & h^i_{\mathrm{NOM}} > 36\,089\ \mathrm{ft}. \end{cases} \tag{21}$$

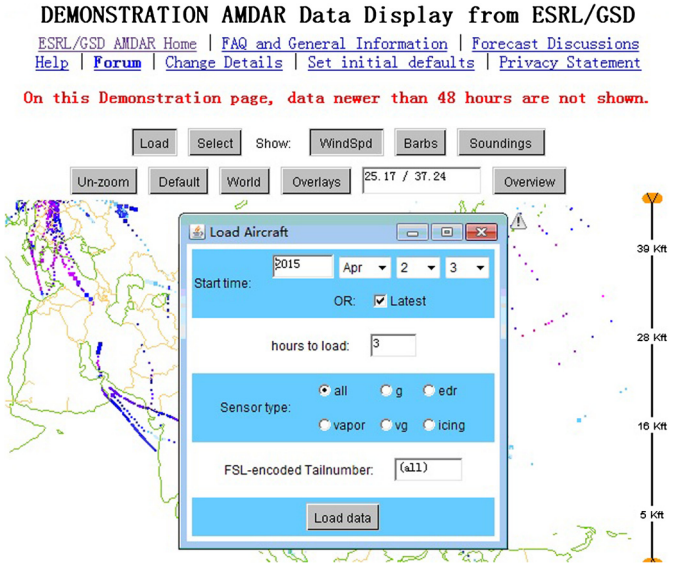

Fig. 13. Example of AMDAR data display.

Table 2
Part of the AMDAR data for the same flight.

Latitude (°)	Longitude (°)	Altitude (ft)	Wind speed (m/s)	Air temperature (°C)
34.4340	108.7690	1300	3	9.0
34.4170	108.7520	2000	9	8.1
34.4170	108.7350	2800	13	5.8
34.4170	108.7350	2900	13	5.3
34.4000	108.7350	3100	13	5.0
34.3830	108.6850	4100	16	2.5
34.3500	108.6520	5700	11	−0.6

The ground speed can then be given by

$$v^i_{\mathrm{GS}} = v^i_{\mathrm{TAS}} \cdot \cos\varepsilon_i + \left(\left(u^i_{\mathrm{FST}}\right)^2 + \left(v^i_{\mathrm{FST}}\right)^2\right)^{1/2} \cdot \cos\alpha_i. \tag{22}$$

Suppose that the horizontal distance between waypoint z^i_{NOM} and z^{i+1}_{NOM} is calculated by Equation (8) and denoted by $d_{i,i+1}$, then the time $\Delta\tau_i$ from waypoint z^i_{NOM} to z^{i+1}_{NOM} can be calculated by

$$\Delta\tau_i = \int_0^{d_{i,i+1}} \frac{\mathrm{d}s}{v^i_{\mathrm{TAS}} \cdot \cos\varepsilon_i + ((u^i_{\mathrm{FST}})^2 + (v^i_{\mathrm{FST}})^2)^{1/2} \cdot \cos\alpha_i}. \tag{23}$$

5. Simulation and discussion

5.1. Simulated case study

As a simulation case study, we considered a flight from Xi'an Xianyang airport (ZLXY) to Jiangxi Changbei airport (ZSCN). The historical AMDAR file acquired from the website of the National Oceanic and Atmospheric Administration (http://amdar.noaa.gov/demo_java/) is shown in Fig. 13.

First, we obtained 548 observation waypoints from the AMDAR data for the same flight on 7 days, and part of the AMDAR data is shown in Table 2.

Only 514 qualified observations were selected and the original flight altitude profiles from h_1 to h_7 are shown in Fig. 14.

Table 3 was obtained by calculating the DSW distance between each flight altitude profile using equation (4). Obviously, the summed value of the DSW distance between h_5 and the others was the minimum. According to equation (5), h_5 is regarded as the nominal flight altitude profile as shown in Fig. 15. The fitting degree for h_5 was calculated as $\gamma(h_5) = 93.23\%$ via equation (6).

Table 3
Distance table obtained by dynamic space warping.

	h_1	h_2	h_3	h_4	h_5	h_6	h_7
h_1	0	5.45	18.65	2.12	4.22	6.45	27.89
h_2	5.45	0	1.89	3.79	0.62	1.31	7.42
h_3	18.65	1.89	0	7.38	3.16	3.59	3.28
h_4	2.12	3.79	7.38	0	2.58	4.83	22.88
h_5	4.22	0.62	3.16	2.58	0	1.43	7.98
h_6	6.45	1.31	3.59	4.83	1.43	0	10.82
h_7	27.89	7.42	3.28	22.88	7.98	10.82	0
Sum of distance	64.78	20.48	37.95	43.58	19.99	28.43	80.27
Fitting degree	78.08%	93.07%	87.16%	85.25%	93.23%	90.38%	72.83%

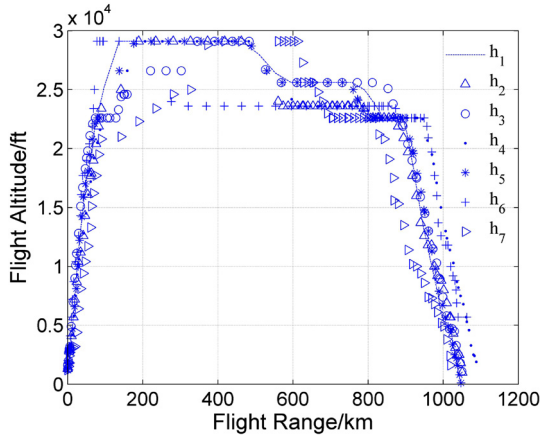

Fig. 14. Diagram showing the original flight altitude profiles.

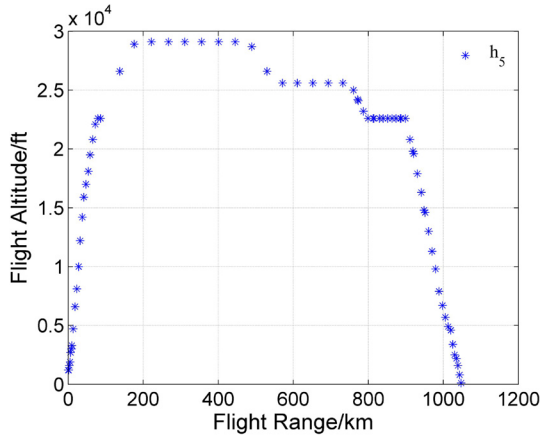

Fig. 15. Diagram showing the nominal flight altitude profile.

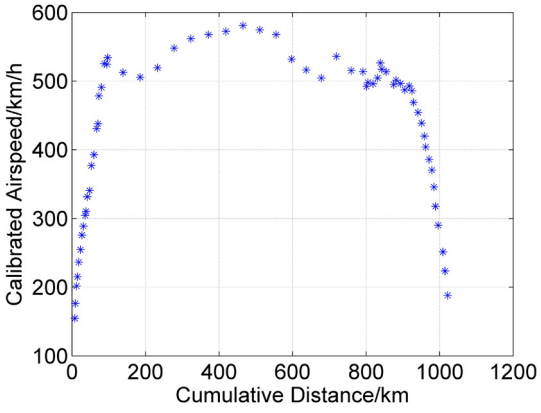

Fig. 16. Diagram showing the nominal calibrated airspeed profile.

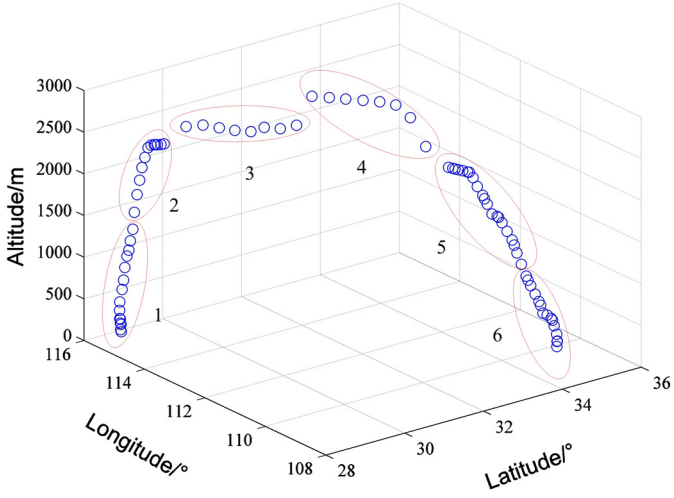

Fig. 17. Illustration of AMDAR observations.

Given the mean earth radius $R_{\mathrm{ME}} = 6\,371\,009$ m and $t_{MSL} = 288.15$ K in equation (8), the nominal calibrated airspeed profile was obtained via equation (10), as shown in Fig. 16.

To verify the accuracy of the strategic 4D trajectory estimation based on the nominal flight profile, we selected two aircrafts from ZLXY to ZSCN on 1/1/2014, where the first from 06:30 to 08:02 was called reference aircraft and the second from 09:08 to 10:30 was called the object aircraft. In total, 73 observations from AMDAR data relayed by the reference aircraft were used to revise the meteorological forecast, while 79 observations from AMDAR data relayed by the object aircraft were used to validate the accuracy of meteorological forecast revision.

We used observations from the reference aircraft to revise the meteorological forecasts from GRIB data. As shown in Fig. 17, 71 observations were divided into six groups to ensure that each tridimensional grid contained sufficient observation waypoints. For example, group 1 comprised 15 observations, as shown in Table 4.

The meteorological forecasts for eight vertices from a tridimensional grid containing group 1 are listed in Table 5, which were acquired from archive datasets ordered from the web site of the European Centre for Medium-Range Weather Forecasts (http://apps.ecmwf.int/datasets/) shown in Fig. 18 and extracted by READ_GRIB, which is a WMO GRIB file reader that can be used to read WMO international exchange GRIB formatted data files into MATLAB.

The Meteorological observations from N_1–N_{15} were used to revise meteorological forecasts for the waypoints in the tridimensional grid composed by M_1–M_8 via Cressman interpolation from equation (12) to equation (17), and the meteorological forecast errors were listed in Table 6.

Table 4
Meteorological observations acquired from AMDAR data.

	Latitude (°)	Longitude (°)	Altitude (m)	Wind direction (°)	Wind speed (m/s)	Air temperature (°C)
N_1	28.851	115.901	121.92	235	2	13.3
N_2	28.851	115.884	335.28	209	1	11
N_3	28.834	115.884	396.24	241	2	10.6
N_4	28.834	115.884	548.64	249	4	10.1
N_5	28.8	115.867	914.4	219	2	8.5
N_6	28.803	115.873	1019.8	175	6	7.9
N_7	28.783	115.834	1280.16	166	12	7.1
N_8	28.816	115.801	1767.84	142	5	5.5
N_9	28.866	115.818	2103.12	197	18	3.5
N_{10}	28.899	115.818	2590.8	185	22	1.9
N_{11}	28.949	115.818	3017.52	185	13	1.8
N_{12}	28.999	115.818	3230.88	216	22	2.5
N_{13}	29.049	115.835	3566.16	221	29	0.4
N_{14}	29.116	115.835	3992.88	224	37	−1.5
N_{15}	29.166	115.852	4632.96	267	24	−5.3

Table 5
Meteorological forecasts from GRIB data.

	Latitude (°)	Longitude (°)	Altitude (m)	Wind direction (°)	Wind speed (m/s)	Air temperature (°C)
M_1	28.5	116.25	5070	223.40	0.89	13.29
M_2	28.5	111.75	5070	258.96	1.12	11.24
M_3	28.5	116.25	120	250.40	4.01	15.47
M_4	28.5	111.75	120	267.36	4.78	14.87
M_5	29.25	116.25	5070	271.79	15.64	−20.87
M_6	29.25	111.75	5070	275.95	16.92	−21.03
M_7	29.25	111.75	120	284.16	26.91	−23.31
M_8	29.25	116.25	120	289.29	24.88	−24.03

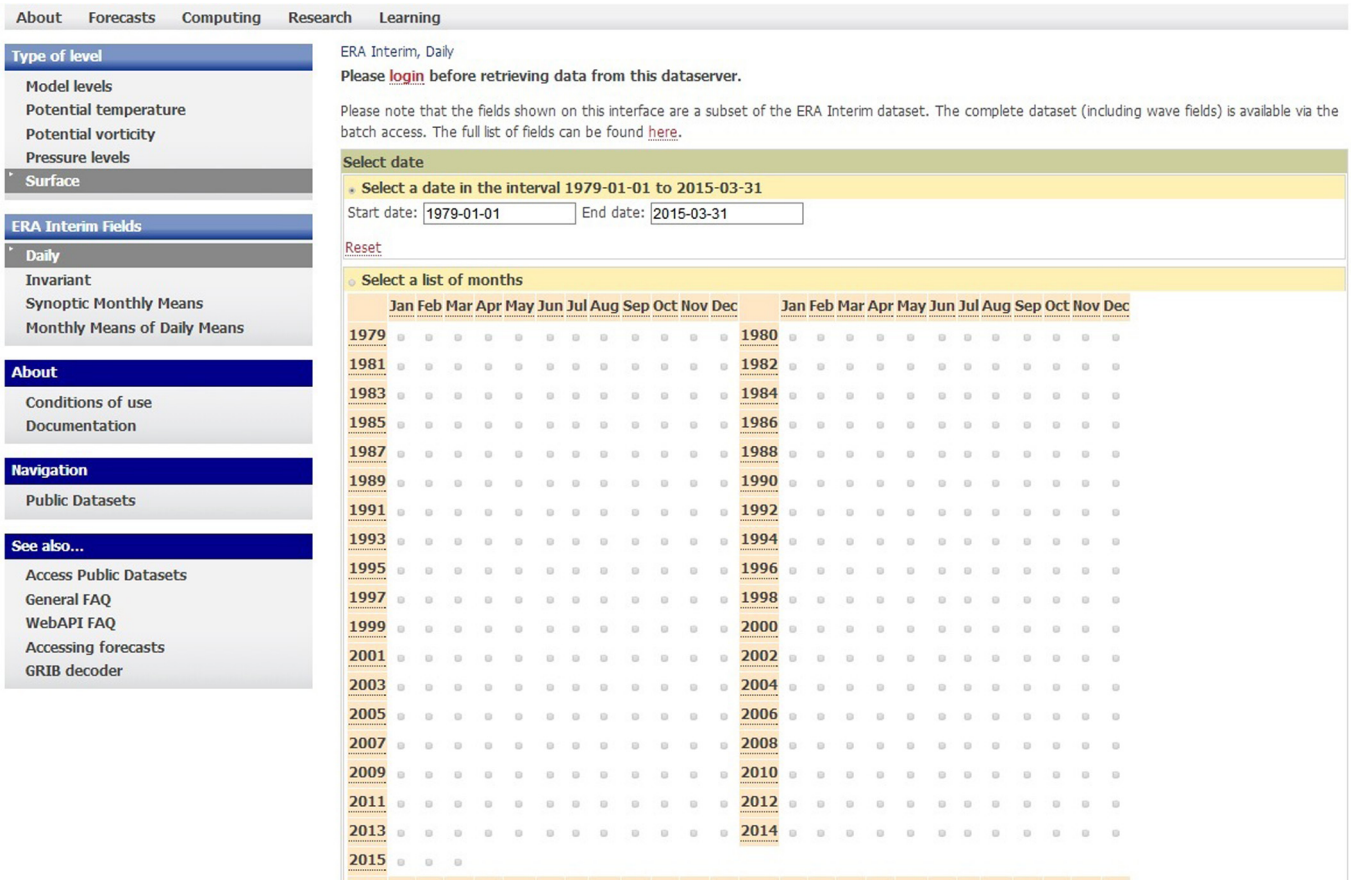

Fig. 18. Interface to select archived datasets.

Table 6
Meteorological forecast errors.

	Wind direction error (°)	Wind speed error (m/s)	Air temperature error (°C)
M_1	−24.57	−0.03	0.89
M_2	80.28	0.01	0.96
M_3	87.64	0.25	−0.20
M_4	90.90	−0.20	0.94
M_5	114.15	1.36	−1.65
M_6	−19.32	1.64	0.44
M_7	105.14	−0.91	−1.96
M_8	92.57	2.34	−2.21

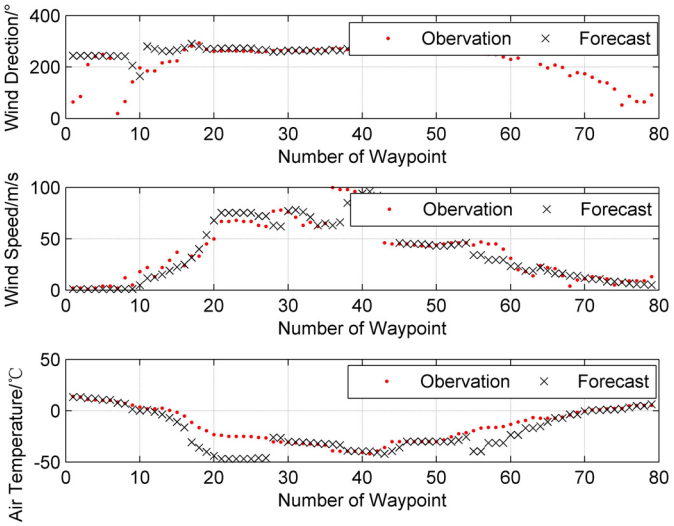

Fig. 19. Comparison of the original GRIB forecasts and AMDAR observations.

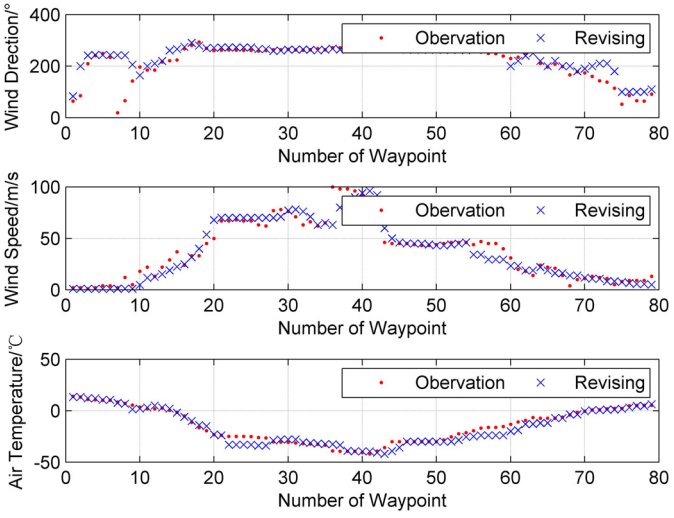

Fig. 20. Comparison of the revised GRIB forecasts and AMDAR observations.

The meteorological forecasts for any other waypoint in nominal fight altitude profile included in the tridimensional grid composed by M_1–M_8 could be calculated via linear interpolation equation (18) and equation (19). Fig. 19 compares the original forecasts from GRIB data and observations from AMDAR data, while Fig. 20 compares the revised forecasts and observations.

After combining the revised airway meteorological forecasts with the nominal flight profile, we determined the times of arrival at given waypoints via equation (23) and the distance from ZSXY for the object aircraft, as shown in Fig. 21.

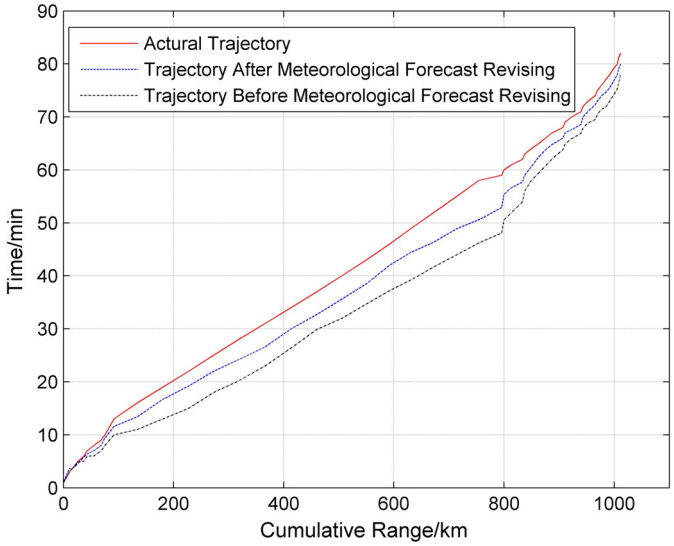

Fig. 21. 4D trajectory obtained by considering the revised airway meteorological forecasts.

5.2. The analysis of the simulation results

The flight altitude profiles varied with the flight intention and the extracted nominal flight altitude profile h_5 shown in Fig. 15 agrees with the typical flight altitude profile shown in Fig. 4. The extracted nominal altitude profile parameters for each stage can be described as follows. The flight climbed from the departing airport elevation directly to 8900 m directly, and then cruised at a flight level of 8900 m and 8100 m. Before approaching it descended to a flight level 6900 m and finally it descended to landing airport's elevation continuously. h_7 was an exceptional sample where the leveling altitude is lower than that of the others, and the sum of the DSW distance between h_7 and the other flight altitude profiles was the maximum. As a result, the fitting degree for h_7 is 72.83%, and thus it was not a representative example. Obviously, number of samples is the key to extract nominal flight altitude profile, if we had utilized more samples, the fitting degree for the extracted nominal altitude profile would have been higher and more representative. To obtain more flight altitude samples, a feasible approach is to combine with other surveillance data from Secondary Surveillance Radar (SSR) or Automatic Dependent Surveillance-Broadcast (ADS-B).

As for nominal airspeed profile shown in Fig. 16, to verify its conformation with the real flight calibrated airspeed plan, we employed flight calibrated airspeed records acquired form an airborne Quick Access Recorder (QAR), as shown in Fig. 22. According to Table 7, we found that the relative errors in the mean airspeed during climbing, cruising and descending state were −7.53%, 0.33% and 4.03%, respectively. Thus, the error in the cruising stage was much less because the duration of this stage was much longer and thus more samples were acquired in this stage compared with the others. However, the errors of nominal airspeed profile are results of two facts: the accuracy of the ground speed calculation was not very high due to the time differences between the two waypoints in the AMDAR data, and there were errors in the meteorological observation from AMDAR data. The most effective way of eliminating this inaccuracy is to introduce QAR data from airlines directly into airspeed profile clustering process, thereby extracting more accurate flight intention.

The mean relative errors before and after revision are shown in Table 8. We revised the original forecasts from GRIB data for the object aircraft and compared with the observations from AMDAR

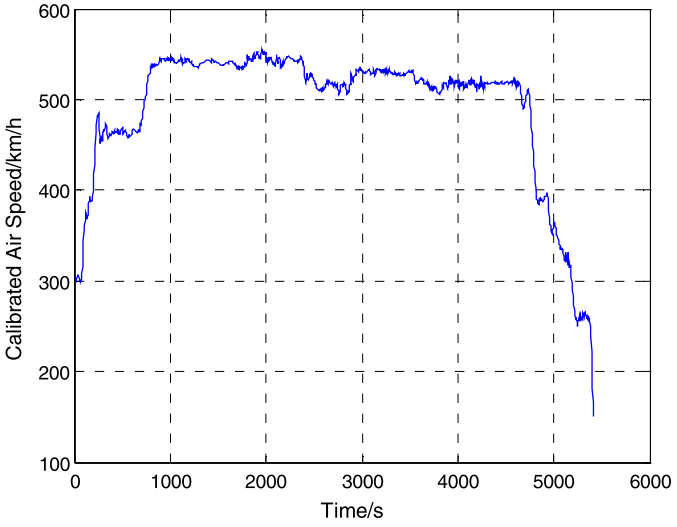

Fig. 22. Diagram showing the flight calibrated airspeed with time acquired from QAR.

Table 7
Mean calibrated airspeed in different flight stage.

Flight stage	Extracted nominal airspeed profile	Calibrated airspeed acquired form QAR	Relative error
Climbing	327.56	354.26	−7.53%
Cruising	523.62	521.88	0.33%
Descending	347.39	333.91	4.03%

Table 8
Comparison of meteorological factors.

Meteorological factors	Mean relative error before revision	Mean relative error after revision
Wind direction	50.84%	28.19%
Wind speed	7.56%	4.32%
Air temperature	16.0%	6.16%

data, the mean relative errors for the wind direction, wind speed, and air temperature decreased from 50.84% to 28.19%, from 7.56% to 4.32%, and from 16.0% to 6.16% respectively. Obviously, the original meteorological forecast errors for the observation waypoints were reduced dramatically. The accuracy was improved by revision except for wind direction because the factors that determine the wind direction in the high altitude airspace are very complex. However, Cressman interpolation is an interpolation method that only considers the distance between observation waypoints and forecast waypoints. Thus, to improve the accuracy of wind direction revision, other nonlinear revision models should be employed to considering driving air flow force, Coriolis force, and air temperature.

We employed 20 waypoints to calculate the relative error in the time of arrival, as shown in Table 9, based on the estimated 4D trajectory in Fig. 21. After applying the revised airway meteorological forecasts to the extracted nominal flight profile, the mean relative error in the time of arrival at the 20 waypoints improved from 23.25% to 11.45%, thereby demonstrating that the flight intention and meteorological factors have the main effects on the accuracy of 4D trajectory estimation. Thus, combining nominal flight profile with revised meteorological forecasts based on observations is a feasible method for improving the accuracy of 4D trajectory estimation.

Table 9
Relative error in the time of arrival before and after revision.

Number	Relative error in time of arrival before revision	Relative error in time of arrival before revision
1	25.00%	12.50%
2	22.22%	11.11%
3	20.00%	6.00%
4	23.08%	10.77%
5	31.25%	16.25%
6	31.58%	12.11%
7	31.82%	12.73%
8	28.00%	12.00%
9	27.86%	13.57%
10	25.81%	14.19%
11	22.35%	11.76%
12	19.19%	11.62%
13	20.00%	11.00%
14	19.30%	10.47%
15	19.13%	8.70%
16	19.80%	9.18%
17	19.81%	10.77%
18	20.00%	11.09%
19	20.34%	12.76%
20	18.47%	10.34%
Average	23.25%	11.45

6. Conclusions

In this study, we proposed a method for extracting the nominal flight profile based on AMDAR data, including extracting the nominal flight altitude profile using the DSW distance algorithm and nominal airspeed profile extraction with the CAS/TAS conversion model. Our simulation case demonstrated that the method extracting nominal flight profile reflected the flight intention and it eliminated the randomness in the trajectory caused by meteorological factors. According to our simulation case, the extracted nominal flight altitude profile agrees with the typical flight altitude profile shown in Fig. 4, and the number of flight profile samples is the key to extract nominal flight altitude profile, if we had utilized more samples, the fitting degree for the extracted nominal altitude profile would have been higher and more representative. However, for extracted nominal airspeed profile, the relative errors in the mean airspeed during climbing, cruising and descending state were −7.53%, 0.33% and 4.03%, respectively. The errors of nominal airspeed profile are results of two facts: the accuracy of the ground speed calculation was not very high due to the time differences between the two waypoints in the AMDAR data, and there were errors in the meteorological observation from AMDAR data.

In addition, we proposed an airway meteorological forecasts revising model, which employs the meteorological observations acquired by reference aircraft to revise those meteorological forecasts related to object aircraft via Cressman interpolation. The revised forecasts can then be used to forecast airway meteorological factors for the object aircraft. According to our simulation case, the mean relative errors for the wind direction, wind speed, and air temperature decreased from 50.84% to 28.19%, from 7.56% to 4.32%, and from 16.0% to 6.16% respectively after revision. Obviously, the accuracy was improved by revision except for wind direction because the factors that determine the wind direction in the high altitude airspace are very complex. However, Cressman interpolation is an interpolation method that only considers the distance between observation waypoints and forecast waypoints. Thus, to improve the accuracy of wind direction revision, other nonlinear revision models should be employed.

After applying the revised airway meteorological forecasts to the extracted nominal flight profile, the estimated 4D trajectory is more accurate and the mean relative error in time of arrival at 20 waypoints improved from 23.25% to 11.45%, thereby demon-

strating that combining the nominal flight profile with revised meteorological forecasts based on observations is a feasible method for improving the accuracy of 4D trajectory estimation. However, there is still plenty of room for improving the accuracy of this method in the future if we consider other operational conditions such as the aircraft performance and conflicts with other aircraft.

Conflict of interest statement

We declare that we have no conflict of interest.

Acknowledgements

This research was supported by National Natural Science Foundation of China (61174180), Jiangsu Union Innovation Fund Projects (BY2012014), and Chinese Postdoctoral Science Foundation (2014M550291).

References

[1] X.P. Lv, General framework of China's new-generation civil aviation ATM system, China Civ. Aviat. 80 (2007) 24–26.
[2] R. Slattery, Y.Y. Zhao, Trajectory synthesis for air traffic automation, J. Guid. Control Dyn. 2 (1997) 232–238.
[3] S.F. Wu, S.F. Guo, Synthesis of aircraft vertical flight profile based on four-dimensional guidance in terminal airspace, Acta Aeronaut. Astronaut. Sin. 14 (1993) 258–261.
[4] A.C. Richard, En route climb trajectory prediction enhancement using airline flight planning information, in: Proceedings of the AIAA Guidance, Navigation, and Control Conference, 1999, pp. 1077–1086.
[5] G. Chester, N.C. William, Using flight manual data to derive aero-propulsive models for predicting aircraft trajectories, in: AIAA' Aircraft Technology, Integration, and Operations (ATIO) 2002 Technical, 2002, pp. 1–7.
[6] C. Wang, J.X. Guo, Z.P. Shen, Prediction of 4D trajectory based on basic flight models, J. Southwest Jiaotong Univ. 44 (2009) 295–300.
[7] X.M. Tang, Y.X. Han, 4D trajectory estimation for air traffic control automation system based on hybrid system theory, Promet Traffic & Transportation 24 (2012) 91–98.
[8] J. Krozel, A. Dominick, Intent inference with path prediction, J. Guid. Control Dyn. 29 (2006) 225–236.
[9] J.L. Yepes, I. Hwang, M. Rotea, New algorithms for aircraft intent inference and trajectory prediction, J. Guid. Control Dyn. 30 (2007) 370–382.
[10] M.A. Konyak, D. Warburton, J. Lopez-Leones, A demonstration of an aircraft intent interchange specification for facilitating trajectory-based operation in national airspace system, in: AIAA Guidance, Navigation and Control Conference and Exhibit, 2008, pp. 1–17.
[11] K. Wu, W. Pan, 4D trajectory prediction model based on data mining, Comput. Appl. 27 (2008) 2637–2639.
[12] M. Gariel, A.N. Srivastava, E. Feron, Trajectory clustering and an application to airspace monitoring, IEEE Trans. Intell. Transp. Syst. 12 (2011) 1511–1524.
[13] Eurocontrol Experimental Centre, User Manual for the Base of Aircraft Data, 2010, pp. 1–56.
[14] C.P. Tino, L.L. Ren, J.B. Clarke, Wind forecast error and trajectory prediction for en-route scheduling, in: AIAA Guidance, Navigation, and Control Conference, 2009, pp. 1–22.
[15] Q.M. Zheng, Y.J. Zhao, Modeling wind uncertainties for stochastic trajectory synthesis, in: 11th AIAA Aviation Technology, Integration, and Operations (ATIO) Conference, 2011, pp. 1–22.
[16] T.G. Reynolds, Y. Glina, S.W. Troxe, M.D. Mcrtland, Wind Information Requirements for NextGen Applications Phase 1: 4D-Trajectory Based Operations (4D–TBO), The National Technical Information Service, 2013, pp. 1–67.
[17] P. Weitz, Determination and visualization of uncertainties in 4D-trajectory prediction, in: Integrated Communications, Navigation and Surveillance Conference, ICNS, 2013, pp. 1–9.
[18] Y.B. Zhu, Y.T. Guo, J. Zhang, A study of AMDAR-based air route meteorological model, Avionics Technol. 40 (2009) 18–23.
[19] J.Q. Zhong, M. Chen, S.Y. Fan, Assimilation application of AMDAR data to the operational NWP system of Beijing, J. Appl. Meteorol. Sci. (2010) 19–28.
[20] S.B. Ding, Flight Performance and Flight Plan, Science Press, Beijing, 2013.
[21] E. Keogh, C.A. Ratanamahatana, Exact indexing of dynamic time warping, Knowl. Inf. Syst. (2005) 358–386.
[22] J.F. Lichtenauer, E.A. Hendriks, M.J.T. Reinders, Sign language recognition by combining statistical DTW and independent classification, IEEE Trans. Pattern Anal. Mach. Intell. 30 (2008) 2040–2046.
[23] J.M. Feng, T.B. Zhao, Y.J. Zhang, Intercomparison of spatial interpolation based on observed precipitation data, Climatic Environ. Res. 02 (2004) 261–277.